Journal of Environment and Earth Science
ISSN 2224-3216 (Paper) ISSN 2225-0948 (Online)
Vol.15, No.5, 2025

Solar quiet Current and Conductivity-Depth Structure of Asia Sub-Region from Magnetic Field Variation at Moderate Solar Activity

Mustapha Abbas[1, *], Arzika Yusuf Koko[1, 4], Mukhtar Mohammad[2], Mukhtar Ibrahim Furfuri[1, 3], Aminu Muhammad[1], Asabe Ibrahim Audu[2] , Mohammed Bello Kaoje[1]

1 Department of Physics, Kebbi State University of Science and Technology, Aliero, Nigeria

2 Department of Physics, Federal University of Agriculture, Zuru,-Kebbi State, Nigeria

3 Department of Physics, Federal College of Education Technical, Gusau, Zamfara State, Nigeria

4 Department of Physics, Federal University of Education, Kotangora, Niger State, Nigeria

* E-mail of the corresponding author: maphysik@yahoo.com

Abstract

The study used some selected magnetic field records to establish the equivalent external and internal ionospheric current system and also profile the conductivity structure beneath the Asian sub-region during the moderate solar quiet year 2012. Spherical harmonic analysis (SHA) was employed to separate the external and internal Sq current and also harmonic coefficients used to probe the conductivity values. The result showed that the month-by-month behavior of the external and internal equivalent current is stronger in local summer months (May-August) and weaker in local winter months (November-February). The current vortex appears earlier in local summer than in local winter months and disappeared in December. In each of the month, the latitudinal position of the internal Sq current vortex appeared at a considerable higher latitude relative to the external. A regression line fitted to the estimated conductivity values gives a profile that starts at 0.02 S/m at a depth of about 30 km and rose gradually to about 0.03 S/m seen at ~120 km depth. Consequently the conductivity profile increases significantly to about 0.07 S/m at depth of about 400 km followed by a sharp steep increase through the transition zone and reached its peak value ~0.3 S/m at depth of about 770 km. An evidence of discontinuity was observed at depth of about 370-440 km and 603-671 km. The sharp steep increase in conductivity profile at depth of about 400 km may be due to phase change of the mantle minerals from olivine to spinel structure.

Keywords: Solar quiet current, Geomagnetic field, Ionosphere, Mantle conductivity

DOI: 10.7176/JEES/15-5-05
Publication date: October 31st 2025

1. Introduction

The daily geomagnetic field variation at the Earth surface has quite a number of sources which are of external and internal origin to the Earth surface Yamazaki and Maute, 2017 and Villier *et al.,* 2017. The field produce by these sources are generally time dependent and changes slowly with latitudes depending on the magnetic activity on the outer space. According to the classical dynamo theory, the main source of the daily geomagnetic field is the electric current flowing at an altitude (90-150 km) in the E-region of the ionosphere generated by the motion of conducting particles across the Earth's main magnetic field, Richmond, 1979. When magnetic disturbances are absent, the current generated is known as solar quiet (Sq) current. The sensitivity of Sq current amplitude to solar activity is different from one season to another such that its strength has an annual variation with higher intensity in summer at mid-latitude region and a semi-annual variation in which it is strongest in equinox at equatorial low latitude, e.g., Matsushit and Maeda, 1965 and Yamazaki and Maute, 2017.The variability of Sq current system has been attributed to variation in the ionospheric conductivity Liu et al., 2021. In a different study, Torta et al., 1997attributed the variability of the Sq current to variation of the tidal and prevailing winds in the upper atmosphere. The equivalent Sq current system during the sunlight hours has two current vortices (one on each hemisphere) centered on the local noon. The current flows in the northern (southern) hemisphere counter-clockwise (clockwise) direction Liu et al., 2021. The fluctuating current induced corresponding currents into the conducting Earth structure. The magnitude, direction and depth at which the induced current penetrate is determine by the effective wavelength of the source current and the distribution of electrically conducting materials within the Earth's interior, Campbell et al., 1998. The primary aim of this study is to investigate the month-by-month behavior of the external and internal Sq current system and to estimate the conductivity profile of the mantle beneath Asia sub-region.

Most previous studies focused on the total Sq current with little or no much information about the external and internal component of the Sq current system and also the electrical conductivity of the Earth mantle. This could be due to the fact that the behavior of the internal Sq current is mainly control by the external Sq current and the electromagnetic induction effect coupled with the complex mathematical procedure required for conductivity profiling. Till now, the characteristics of the external and internal Sq current in the East Asia sub-region and the upper mantle conductivity are not fully understood yet. In this present work, we used set of geomagnetic field during moderate solar activity year 2012 to study the variability features of the external and internal Sq current and the upper mantle conductivity in East Asia sub-region. In view of this, the data and analysis procedure are explained in section 2. The result and discussion are given in section 3 and we draw a logical conclusion in section 4.

2. Data and Method of Analysis

2.1 Sources of Data

The magnetic field data set used in this study are from the International Real-time Magnetic Observatory Network (INTERMAGNET) for the year 2012 which are accessible at https://imag-data. bgs.ac.uk /GIN _V1/GINForms2. The observatories had their sample records available in minute average values and the original recordings of the field across all the stations were in Universal time (UT) and are all converted to local time (LT). The intermagnet data are recorded as orthogonal north, east and vertically downward components field as X, Y and Z and the X and Y are transformed to their respective northward (H) and eastward (D) coordinate system using the relation given in Campbell, 2003. The magnetic stations used span from the magnetic equator to high latitude region and table 1.0 shows the list of the stations and their coordinates used in the analysis. In the data selection, the first criteria adopted to ensure good and quality data are used was to select days in which the geomagnetic disturbance index Kp values are not greater than 3 as earlier suggested by Campbell, 2007. These groups of quiet days were obtained as published by World Data Centre Kyushu at https://wdc.kugi.kyoto-u.ac.jp/wdc/Sec3.html. These days have least solar-terrestrial magnetic disturbances, thus represent the Sq fields generated by dynamo currents in the E region of the ionosphere.

Table 1.0 list of stations and their coordinates used in the study

Name	Code	GG. Lat (°N)	GG. Lon. (°E)	GM. Lat (°N)
Dalat	DLT	11.94	108.48	2.60
Phu thuy	PHU	21.03	105.97	10.78
Zhaoqing	GZH	22.00	112.45	12.74
Kanoya	KNY	31.42	130.88	20.50
Kokioka	KAK	36.23	140.19	27.37
Beijing Ming Tomb	BMT	40.30	116.20	30.04
Memenbetsu	MMB	43.91	144.15	35.35
Changchum	CNH	44.08	124.86	31.00
kutsk	IRT	52.27	104.45	41.84
Paratunka	PET	53.97	158.25	46.10
Magadan	MGD	60.05	144.19	53.49

2.2 Method of Data Analysis

The analysis started by assuming that the Earth rotates around the sun and the magnetic observatories across the latitudes are riding with the Earth under a fixed subsolar ionospheric current system. These magnetic observatories picked the behavior of the field source current and the current induced into the conducting Earth. The variations of Sq field at any of the latitude in 24 hours represent the measured field through 360° of a sphere. Campbell et al. 1998 called this technique "cloning" a sphere from a longitudinal "slice" sample.

Next, a hemispheric mirror modeling technique that utilizes the field values of the hemisphere which is of primary interest to create a secondary hemisphere in the opposite hemisphere was done. This was achieved on the assumption that the variation of H-field at the secondary hemisphere is similar to the primary hemisphere but its D and Z component are caused to be oppositely directed by simply changing the appropriate sign of the two (D and Z) components so as to conform to the reversed source-current vortex as suggested by Campbell et al., 1998. In the mirror hemisphere, the variations of the Sq field of the H, D and Z components of the primary hemisphere were shifted by 6 months in such a way that the summer hemisphere of the primary stations corresponds to the winter hemisphere of the secondary hemisphere. Also, for each particular day the harmonic coefficients was generated with field values at 2.5^0 latitude increments, pole to pole as input parameter to the spherical Harmonic analysis (SHA) analysis. At this particular stage, a complete sphere consisting of the primary and secondary hemisphere has been successfully created and the outcome of the analysis was strictly assigned to the primary region of interest.

Previous studies on the spectral contributions to the Sq field reveal that only the 24-, 12-, 8- and 6-hr harmonics components are great enough to make significant contribution to the Fourier analysis. Their greater magnitudes are associated with the effect of the Earth's rotation and not on the characteristics of the signal at any given day. On this note, the 24-, 12-, 8-, and 6-hr monthly Fourier sine and cosine coefficients for each station and component from the detrended Sq field records were determined. The annual and semi-annual Fourier components of 12 (months) daily coefficients at each 2.5° magnetic latitude increments from the geomagnetic equator to north and south poles were determined by Campbell and Schiffmacher, 1985. The obtained Fourier coefficients were then stored in a file and thus represent the year's Sq field variations for each component. For any geomagnetic component W (H, D and Z), the Sq field could be constructed from;

$$\Delta W = \sum_{m=1}^{4}\{C_m \cos(15mt) + S_m \sin(15mt)\} \quad (1)$$

where ΔW represent the changes for the H, D or Z field component from the daily mean value of the surface field records. The t is the local time (LT) in hours at the stations, while C_m and S_m are the cosine and sine amplitude coefficients as given in the equation below:

$$C_m = A_m^0 + \sum_{Q=1}^{2}\{A_m^{AQ}\cos(30MQ) + B_m^{AQ}\sin(30MQ)\} \quad (2)$$

$$B_m = B_m^0 + \sum_{Q=1}^{2}\{A_m^{BQ}\cos(30MQ) + B_m^{BQ}\sin(30MQ)\} \quad (3)$$

where m is the order from 1-4 for the 24,-, 12-, 8-, and 6-hours spectral components. Q is 1 for annual and 2 for semi-annual, while M is the decimal month (represented as 0.00 for January 1 and 12.00 for December 31). The As and Bs are the Fourier amplitude coefficients and the mainline letters are the annual and semi-annual coefficients. Any linear trend on the recorded Sq field variation that will introduce some errors in the sinusoidal amplitude coefficients was removed before the Fourier analysis was performed. The file containing each of the 40 Fourier coefficients representing each of the three orthogonal field directions were carefully arranged according to geomagnetic latitudes of the stations used in the analysis for smoothing. The global observations of Sq fields are more symmetric with respect to geomagnetic axis than the geographic and this cause the SHA coefficients series for the Sq to converge more easily and rapidly with geomagnetic expansion. Therefore, the analysis in this study will proceed with the geomagnetic coordinate system.
The determination of the Sq field V shows that most of the contributions come from the internal part of the magnetic potential function expansion. The magnetic potential of the quiet field obtained from the daily mean values recorded in universal time (UT) from the external source current and the internally induced current is expressed as:

$$V_{ext} = R_E \sum_{n=1}^{\infty}\left(\frac{r}{R_E}\right)^{n} \sum_{m=0}^{n}[a_n^{me}\cos(m\emptyset) + b_n^{me}\sin(m\emptyset)]\, P_n^m(\cos\theta) \quad (4a)$$

$$V_{int} = R_E \sum_{n=1}^{\infty}\left(\frac{R_E}{r}\right)^{n+1} \sum_{m=0}^{n}\left[a_n^{mi}\cos(m\emptyset) + b_n^{mi}\sin(m\emptyset)\right] P_n^m(\cos\theta) \quad (4b)$$

Where θ, a, r, Φ represent geomagnetic colatitude, geocentric distance, Earth's radius and local time of the station. It is clear from equation 4a and 4b that two magnetic potential components are attributed to external and internal sources. The external magnetic potential (V_{ext}) increases with increasing r-indication of increase field strength as the height increases from the surface. Conversely, the internal magnetic field potential (V_{int}) increases with decreasing r-indication of increase field strength with depth from the ground. The a_n^{me}, b_n^{me} and a_n^{mi}, b_n^{mi} correspond to the Gauss coefficient with e and i indicating external and internal field sources. It is conspicuously seen in equation 4a and 4b that the longitudinal dependence of both magnetic field potential are given by Fourier series, while its latitudinal dependence is represented by a series of Schmidt quasi-normalized associated Legendre functions $P_n^m(\cos\theta)$. This function can be estimated using the following recursive formula as provided in Campbell, 2003:

$$R_n^m = \sqrt{n^2 - m^2} \quad (6a)$$

$$P_0^0 = \cos(\theta) = 1;\ P_1^0(\cos\theta) = (\cos\theta);\ P_1^1(\cos\theta) = \sin(\theta) \quad (6b)$$

$$P_n^m(\cos\theta) = \sqrt{\frac{2m-1}{2m}}\sin(\theta)P_{m-1}^{m-1}\,;\,(\cos\theta)\,P_{m-1}^{m-1}\,;\ for\ m>1, n=m \tag{6c}$$

$$P_n^m(\cos\theta) = \frac{(2n-1)\cos\theta\ P_{n-1}^m - R_{n-1}^m - P_{n-2}^m}{R_n^m}\ for\ n > m \tag{6d}$$

$$\frac{dP_n^m}{d\theta} = \frac{n\cos\theta P_n^m(\cos\theta) - R_n^m - P_{n-1}^m(\cos\theta)}{\sin\theta}(except\ for\ \theta = 0\ or\ 180°) \tag{6e}$$

Equation (6e) is undefined at the poles ($for\ \theta = 0\ or\ 180°$).

To determine the spherical harmonic Gauss coefficients, the following values were first obtained:

$$a_n^m = \frac{2n+1}{4n(n+1)}\left(\sum_0^{180} X_c^m \frac{dP_n^m}{d\theta}\sin\theta + Y_s^m\, mP_n^m\right)\Delta\theta \tag{7a}$$

$$b_n^m = \frac{2n+1}{4n(n+1)}\left(\sum_0^{180} X_s^m \frac{dP_n^m}{d\theta}\sin\theta + Y_c^m\, mP_n^m\right)\Delta\theta \tag{7b}$$

$$C_n^m = \frac{1}{4}(2n+1)\sum_0^{180} Z_c^m P_n^m \sin\theta\,\Delta\theta \tag{7c}$$

$$d_n^m = \frac{1}{4}(2n+1)\sum_0^{180} Z_s^m P_n^m \sin\theta\,\Delta\theta \tag{7d}$$

Where X_c^m and X_s^m represent the cosine and sine coefficients of the Fourier component m of the northward (ΔH) field change at colatitude (θ). The $\Delta\theta$ in these equations is the step increment which is equivalent to 2.5^0 ($\Delta\theta = 2.5^{\circ}$) used in the analysis. θ is the geomagnetic colatitude.

The spherical harmonic Gauss coefficient for the external and internal source field is then computed using the equations below:

For the external part

$$a_n^{me} = \frac{[(n+1)a_n^m + C_n^m]}{2n+1} \tag{8a}$$

$$b_n^{me} = \frac{[(n+1)b_n^m + d_n^m]}{2n+1} \tag{8b}$$

The internal part is given as;

$$a_n^{mi} = \frac{[na_n^m - C_n^m]}{2n+1} \tag{8c}$$

$$b_n^{mi} = \frac{[nb_n^m - d_n^m]}{2n+1} \tag{8d}$$

The potential function was separated into external and internal source contributions. With reference to Gauss coefficients, the external fields in the orthogonal directions may be reconstructed from the external spherical harmonic analysis as series of Fourier cosine and sine of the terms:

$$X_c^m(\theta) = \sum_{n=m}^{12} a_n^{me}\frac{dP_n^m}{d\theta} \tag{9a}$$

$$X_s^m(\theta) = \sum_{n=m}^{12} b_n^{me}\frac{dP_n^m}{d\theta} \tag{9b}$$

$$Y_c^m(\theta) = -\frac{m}{\sin\theta}\sum_{n=m}^{12} b_n^{me}\frac{dP_n^m}{d\theta} \tag{9c}$$

$$Y_s^m(\theta) = -\frac{m}{\sin\theta}\sum_{n=m}^{12} a_n^{me}\frac{dP_n^m}{d\theta} \tag{9d}$$

$$Z_c^m = \sum_{n=m}^{12} na_n^{me}\,P_n^m \tag{9e}$$

$$Z_s^m = \sum_{n=m}^{12} nb_n^{me}\,P_n^m \tag{9f}$$

where X_c^m, Y_c^m and Z_c^m are the cosine coefficients of the external orthogonal field components and X_s^m, Y_s^m and Z_s^m are the sine coefficients. For the internal horizontal component the e may be replaced by i and its vertical internal component is expressed as:

$$Z_c^m(\theta) = -\sum_{n=m}^{12}(n+1)a_n^{mi} P_n^m \quad (10a)$$
$$Z_s^m(\theta) = -\sum_{n=m}^{12}(n+1)b_n^{mi} P_n^m \quad (10b)$$

The sphere in which the spherical harmonic analysis is carried out was spherically created to accommodate the boundary conditions of the Gauss method.

The equivalent current function $J(\Phi)$ in Amperes (A) for any hour of the day $\Phi/_{15}$ is expressed as:

$$J(\Phi) = \sum_{m=1}^{4}\sum_{n=m}^{12}\{U_n^m \cos(m\Phi) + V_n^m \sin(m\Phi)\}P_n^m \quad (11)$$

The external current is expressed by:

$$U_n^m = -K\left[\frac{2n+1}{n+1}\right]a_n^{mi}\left(\frac{a}{R}\right)^n \quad (12a)$$

$$V_n^m = -K\left[\frac{2n+1}{n+1}\right]b_n^{mi}\left(\frac{R}{a}\right)^{n+1} \quad (12b)$$

Where $K = \frac{5R}{2\pi}$ and R is the Earth radius given in kilometers, a is the radius of the sphere of the equivalent current location. Throughout the study, a is assumed to be approximately equal to R so that the ration $\frac{a}{R}$ and $\frac{R}{a}$ becomes 1 and the factor was omitted.

2.3 Conductivity of the upper mantle

The set of equations for profiling the conductivity with a transfer function equivalent to a substitute conductor was earlier provided by Schmucker, 1970. These equations required external and internal spherical harmonic coefficients at a given location as input parameters. Later, Campbell and Anderssen, 1983 modify Schmucker's transfer function. The generalized form of Schmucker's transfer function C_n^m as modify by Campbell and Anderssen is expressed as;

$$C_n^m = Z - iP \quad (13)$$

The transfer function for a substitute conductor given in equation (13) has a complex number in which the real (Z) and the imaginary (P) part are expressed as:

$$Z = \frac{R}{n(n+1)}\left\{\frac{A_n^m[na_n^{me}-(n+1)a_n^{mi}]+B_n^m[nb_n^{me}-(n+1)b_n^{mi}]}{(A_n^m)^2+(B_n^m)^2}\right\} \quad (14a)$$

$$P = \frac{R}{n(n+1)}\left\{\frac{A_n^m[nb_n^{me}-(n+1)b_n^{mi}]-B_n^m[na_n^{me}-(n+1)a_n^{mi}]}{(A_n^m)^2+(B_n^m)^2}\right\} \quad (14b)$$

The R that appeared in the equation is the radius of the Earth expressed in kilometers; hence the Z and P are expressed in kilometers. The coefficient A_n^m and B_n^m are obtained using the spherical harmonic coefficients for the external and internal field given below;

$$A_n^m = a_n^{me} + a_n^{mi} \quad (15a)$$
$$B_n^m = b_n^{me} + b_n^{mi} \quad (15b)$$

For each (m,n) set of spherical harmonic coefficients, the depth (in km) to the uniform substitute was estimated using the relation

$$d_n^m = Z - P \quad (16a)$$

And has a substitute –layer conductivity (S/m) given by;

$$\sigma_n^m = \frac{5.4 \times 10^4}{m(\pi P)^2} \quad (16b)$$

The ratio of the internal to the external components of the quiet field variation S_n^m is given as;

$$S_n^m = u + iv \quad (17a)$$

Where

$$u = \left[\frac{(a_n^{me})(a_n^{mi})+(b_n^{me})(b_n^{mi})}{[(a_n^{me})]^2+[(b_n^{me})]^2}\right] \quad (17b)$$

$$v = \left[\frac{(b_n^{me})(a_n^{mi})-(a_n^{me})(b_n^{mi})}{[(a_n^{me})]^2+[(b_n^{me})]^2}\right] \quad (17c)$$

The validity of equation (**a**) and (**b**) is bounded by three conditions: the first condition is given by;

$$0° = arg(C_n^m) \geq -45°; \quad (18a)$$

The second condition is that

$$80° = arg(S_n^m) \geq 10.5°; \quad (18b)$$

The third is that the SHA amplitudes (equation **12**) not be small because the relative error in the SHA coefficients increases with decrease in amplitudes of the coefficients. Hence the amplitude is set at;

$$[(A_n^m)^2 + (B_n^m)^2]^{0.5} \geq G_m \quad (18c)$$

3. Results and Discussion

Figures 1 and 2 show the month-by-month equivalent external and internal Sq current system during moderate solar activity year 2012. It is obvious from these figures that the external and internal equivalent currents are characterized by a single daytime current vortex at mid-latitude that appears stronger in northern summer months (May-August) and weaker in northern winter (November-February). The maximum intensity of the external current reached ~12.6 × 10^4A in June and its minimum ~4.4 × 10^4A is seen in November. The differences in the magnitude between the external and internal Sq current reflect the direct effect of solar activity. The likely phase difference between the external and internal Sq current may result from the neutral wind and electromagnetic induction effect. The internal Sq current has its maximum amplitude value ~-6.2 × 10^4A in June and its minimum - ~2.2 × 10^4A appeared in November.

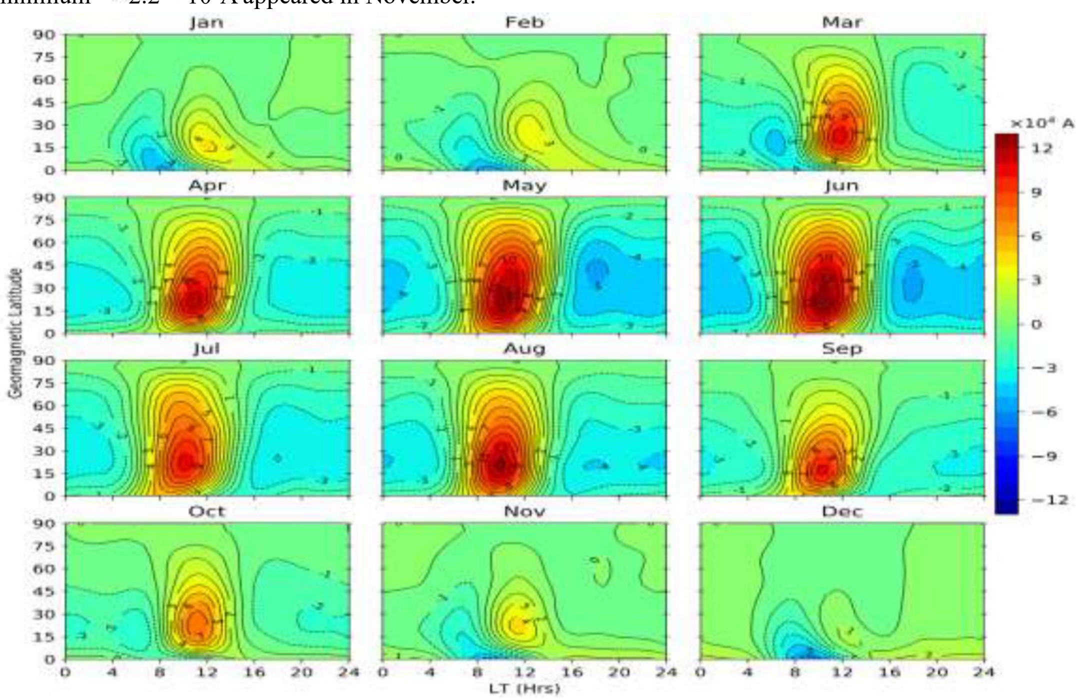

Figure 1 Monthly external Sq current system during moderate solar activity year 2012

The structure and intensity of the Sq current are primarily controlled by the neutral tidal winds and the conductivity in the dynamo region of the ionosphere. Modeling the Sq current system at different solar epoch Takeda et al., 1986 found that changes in ionospheric conductivity cause a corresponding change in the Sq current intensity. This accounts for the maximum intensity of the Sq current system observed in northern summer month (June) of the present study. Apart from the intensity of the external Sq current, the latitudinal position of the current vortex shows that it varies from one month to the other. For example, the latitudinal position of the external Sq current vortex ranged between 23° and 25° conspicuously seen between April to August as depicted in Figure 1. During these periods, the internal Sq current vortex moves poleward relative to the external vortex (see Figure 2). It ranged between 25° and 28° latitude seen between April to September as illustrated in Figure 2. In each month, the latitudinal position of the internal Sq current vortex appeared at relatively higher latitude to the external. Figures 1 and 2 also show that the current vortex appear earlier in local summer months (May-August) than in local winter months (November-February). This variation in the position of the Sq foci has been largely attributed to interhemispheric field-aligned current (IHFACs). Previous studies have earlier suggested that the field-aligned current of the current vortex produce an eastward geomagnetic field that advances the equivalent current vortex in the summer hemisphere and delays the vortex in the winter hemisphere Fukushima 1979. The consequences is that the intensity of the Sq current vortex appears at earlier local time in summer than in winter as obvious in Figures 1 and 2 of the present study. This could be the main reason for the Sq current whorl appearing at later hour of the day in northern winter months.

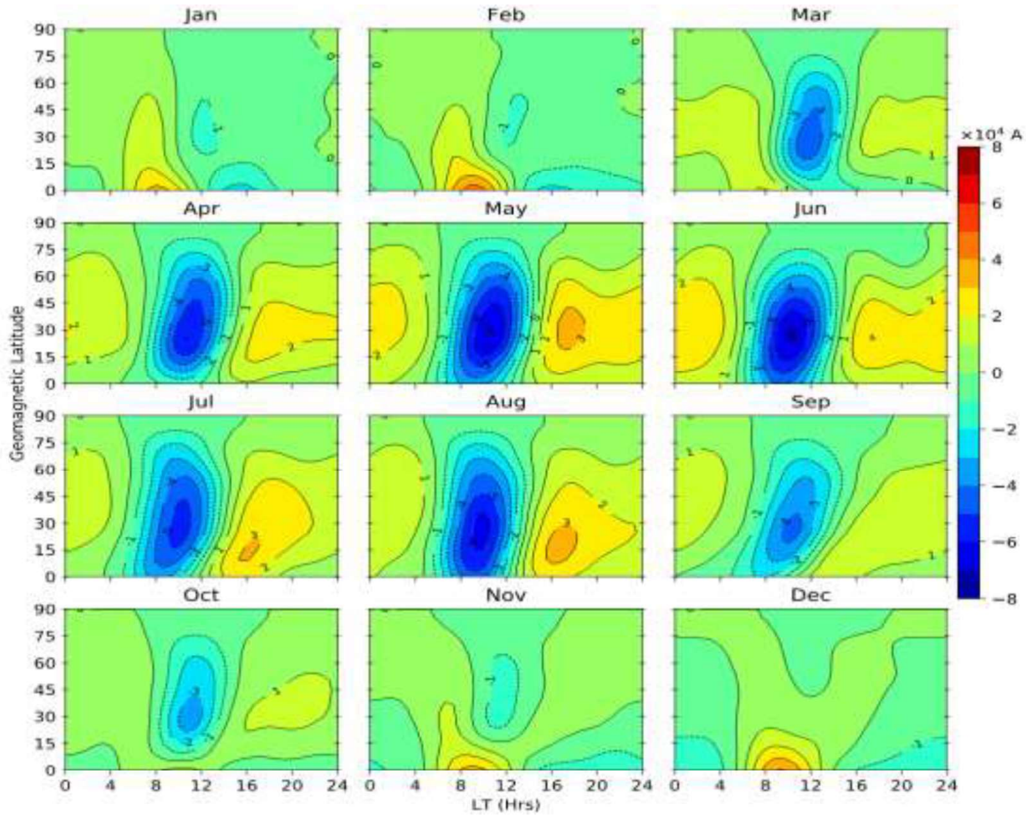

Figure 2.0 Monthly internal Sq current during the moderate solar activity year 2012

During times when the external Sq current was minimum in northern winter, the daytime current in November appears very weak with its vortex at considerable lower latitude (25°) and disappeared in December. The internal Sq current vortex was also observed to disappear in December. This implies that the disappearance of Sq vortex is a consequence of weaker daytime Sq current. This result is in sharp contrast with the earlier findings by Matsushita and Maeda, 1965 that did not observed any disappearance of the Sq vortex focus in their winter months. However, the present result is consistent with the India-Siberia region reported by Campbell and Schiffmacher, 1985. These authors observed disappearance of Sq vortex focus in their winter months. In a similar study by Arora et al., 1995, they found that for the Central Asia Sq focus vortex magnitude to reach about 16.8 x 10^4A in June and July and virtually disappeared in December and January. The disappearance of Sq current vortex particularly in winter months indicates the existence of significant changes in the summer-winter variation pattern of the Sq current system.

Figures 3 show the mantle electrical conductivity-depth profile of Asia sub-region during moderate solar activity year 2012. The blue dotted points are the computed conductivity values. The solid line is the locally weighted regression fitting to the conductivity values computed using the best Lowess technique. A small group of about 3 conductivity values at depth range between 200 and 400 Km are observed in Figure 3. It is not certain whether these are real values or outliers or perhaps there are times when the varying source Sq field is inducing a response from a small scale, high conductivity anomaly at these locations. Similar effect was earlier observed in the India-Siberia region by Cambell and Schiffmacher, 1988. Apart from these small groups of conductivity values, generally the scattered points are much concentrated within the first few kilometers down to a depth of about 450 km and with increasing depth, the density of the scattered points decreases to a depth of about 770 km.

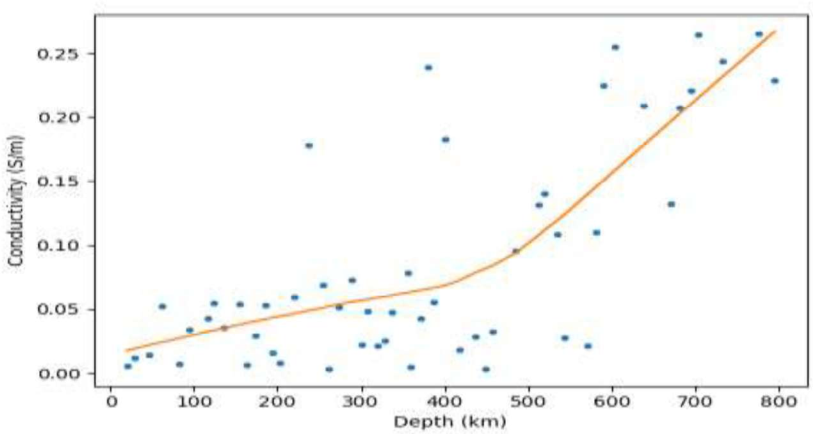

Figure 3 Mantle electrical conductivity-depth profile computed from the monthly spherical harmonic analyses of the Sq fields applied to the equivalent substitute conductor technique. The points that is indicated by • the computed values while the solid line through the points is a locally weighted regression fitting of the computed conductivity values.

These points resulted from series of factors among them includes; error incurred from the field measurements, error from spherical harmonic analysis (SHA) fitting, various sources of currents. The noise in the original data and the effect of lateral inhomogeneity also constitute an error that is very difficult to evaluate accurately, hence what could actually be termed an error is in the measurement of the regression fitting for the scattered conductivity values. It is obvious from both Figure 4 that the profile shows downward increase in conductivity with depth from the crustal surface deep down into the lower mantle in consistent with earlier result of Campbell et al., 1998 that observed conductivity profile to the lower mantle depth beneath Australian region. This downward increase in the conductivity profile is no surprise since for a given Earth's interior the temperature increases with depth hence it is expected for the electrical conductivity to increase accordingly. The gradual increase at depth range between 30 and 120 km indicate the existence of weak conductivity zone. This observation is in Sharp contrast with the South American sector that showed highest conductivity profile at this depth range suggesting lateral inhomogeneity between the continents. However, the present result is Consistent with African observation by Obiora et al., 2015 and also Malaysian region by Abidin et al., 2017. Since the electrical conductivity within few kilometers of the crust depends on the amount of interstitial water that is present, it is likely the weak conductivity may be due to dehydration of the crust through metamorphic process as earlier identified by Ohtani and Sakai, 2008. A sudden increase in conductivity from 0.03 to 0.04 S/m at depth range between 120 and 270 km correspond to the asthenosphere with global seismic low velocity and high electrical conductivity, e.g Dziewonski and Anderson, 1981. A sharp steep increase in conductivity was observed at depth of about 400 km with corresponding magnitude of 0.07 S/m and increases steeply to about 0.15 S/m at depth of 600 km and continued until it reached about 0.3 S/m at depth of 770 km with no indication of leveling off. The sharp steep increase at depth of 400 km may be due to phase change of the mantle materials from olivine to spinel structure as earlier as earlier discussed by research workers e.g., Campbell and Schiffmacher, 1988. The high electrical conductivity profile at depth between 400 and 600 km correspond to the mantle transition zone identified with high electrical conductivity, e.g., Ohtani and Sakai, 2008. The mantle transition zone has been identified as the most likely important water reservoir on Earth due to its ability to store water content of more than 2 wt%, Katsura and Ito, 1989. The enhanced conductivity profile in the transition may likely be influence by the presence of water. The discontinuity profile observed at 370–440 km is likely associated to the transformation of α-phase of olivine to β at high temperature and pressure, Ito and Takahashi, 1989 while the dissociation of γ is ascribed to the seismic discontinuity at 603–671 km, Ito and Takahashi, 1989. The γ-phase split into perovskite and magnessiowustite at the transition zone and even beyond, Chandrasekhar, 2011..

4. Conclusion

The records of the geomagnetic field are used to estimate the variability features of the external and internal Sq current and conductivity profile beneath the Asia sub-region during period of moderate solar activity year 2012. The main findings from the study are summarized below:

1. The monthly behavior of the external and internal Sq current system appears stronger in local summer months (May-August) and weaker in local winter months (November-February).
2. The differences in the intensity of the external and internal Sq current reflect the direct effect of solar activity.
3. The internal Sq current vortex consistently appears more poleward at a range 25^0 and 28^0 latitude relative to the external focus seen around 230 and 250 latitude during the northern summer months (April-September).
4. The external and internal Sq current vortex consistently appeared earlier in northern summer months relative to the northern winter months (November-February) which may likely be influenced by the inter-hemispheric field-aligned current (IHFACs).
5. The disappearance of the external and internal Sq current vortex occurred during the northern winter month (December). The disappearance of Sq current vortex particularly in winter months indicate significant depression in the current intensity.
6. An evidence of discontinuity was observed at depth of about 370-440 km and 603-671 km. The sharp steep increase in conductivity profile at depth of about 400 km may be due to phase change of the mantle minerals from olivine to spinel structure.

References

Abidin, Z..Z., Jusoh, M. H., Abbas, M, and Yoshikawa, A. (2017). Application of solar quiet (Sq) current in determining mantle conductivity-depth structure in Malaysia, *J. Atm. Sol.Terr. Phys.*

Arora, B. R., Campbell, W. H., and Schiffmacher, E. R. (1995). Upper mantle electrical conductivity in the Himalayan region. *J. Geomagn. Geoelectr*. 47, 653–665.

Campbell, W. H., and Anderssen, R. S. (1983). Conductivity of the sub-continental upper mantle: an analysis using quiet-day geomagnetic records of North America. *J. Geomagn. Geoelectr*. 35, 367–382.

Campbell, W. H., and Schiffmacher, E. R., (1985). Quiet ionospheric currents of the Northern Hemisphere derived from geomagnetic field records. *J. Geophys. Res. Space Phys.* 90, 6475–6486.

Campbell, W. H., Schiffmacher, E. R. (1988). Upper mantle electrical conductivity for seven subcontinental regions of the Earth. *J. Geomagn. Geoelectr*. 40, 1387–1406.

Campbell, W. H (1997). Introduction to Geomagnetic fields. Cambridge University Press, New York.

Campbell, W. H., Barton, C. E., Chamalaun, C., and Welsh, W. (1998). Quiet-day ionospheric currents and their applications to upper mantle conductivity in Australia. *Earth Planets Space,* 50, 347–360.

Campbell, W. H (2003). Introduction to Geomagnetic fields. Second ed. Cambridge University Press, New York.

Chandrasekhar, E. (2011). Regional electromagnetic induction studies using long period geomagnetic variations. In: Petrovsky, E., Herrero-Bervera, E., Harinarayana, T., Ivers, D. (Eds.), The Earth's Magnetic Interior, Dordrecht, Heidelberg, London, New York, vol. 1. Springer, pp. 31–42.

de Villiers, J. S., Kosch, M., Yamazaki, Y., & Lotz, S. (2017). Influences of various magnetospheric and ionospheric current systems on geomagnetically induced currents around the world. *Space Weather*, *15*(2), 403-417.

Dziewonski, A. M., and Anderson, D. L. (1981). Preliminary reference Earth model. *Phys. Earth planet* 25, 297–356.

Fukushima, N. (1979). Electric potential difference between conjugate points in middle latitudes caused in the ionosphere. *J. Geom. Geo-electr*. 31, 401–409.

Ito, E., and Takahashi, E. (1989). Post-spinel transformations in the system Mg_2SiO_4-Fe_2SiO_4 and some geophysical implications. *J. Geophys. Res.* 94, 10637–10646.

Katsura, T., and Ito, E. (1989). The system Mg_2SiO_4-Fe_2SiO_4 at high pressures and temperatures: precise determination of stabilities of olivine, modified spinel and spinel. *J. Geophys. Res*. 94, 15663–15670.

Liu, X., Han, P., Hattori, K., Chen, H., Yoshino, C., Zhao, X., ... & Lei, Y. (2021). Seasonal variation characteristics of geomagnetic Sq external and internal equivalent current systems in East-Asia and

Oceania regions. *Journal of Geophysical Research: Space Physics*, *126*(3).

Liu, H., Yamazaki, Y., & Lei, J. (2021). Day-to-Day variability of the thermosphere and ionosphere. *upper atmosphere dynamics and energetics*, 275-300.

Matsushita, S., and Maeda, H. (1965). On the geomagnetic solar quiet daily variation field during the IGY. J. Geophys. Res. 70, 2535–2558

Obiora, D. N., Okeke, F..N., and Yumoto, K.. (2015). Electrical conductivity of mantle in the North Central region of Nigeria. *J. Afr. Earth Sci.* 101, 274–281

Ohtani, E., and Sakai, T. (2008). Recent advances in the study of mantle phase transitions. *Phys. Earth Planet. In.* 170, 240–247.

Richmond, A. D. (1989). Modeling the ionosphere wind dynamo: a review. quiet daily geomagnetic fields. *Pure Appl, Geophys*. 131, 413–435.

Schmucker, U. (1970). An introduction to induction anomalies. J. Geomagn. Geoelectr. 22, 9–33.

Takeda, M., Yamada, Y., and Araki T. (1986). Simulation of ionospheric currents and geomagnetic field variations of Sq for different solar activity. *J. Atmos. Terr. Phys.,* v.48, pp: 277–287.

Torta, J. M., Curto, J. J., Bencze, P. (1997). Behavior of the quiet day ionospheric current system in the European region. *J. Geophys. Res*.102, 2483–2494.

Yamazaki, Y., and Maute, A. (2017). Sq and EEJ-A review on the daily variation of the geomagnetic field caused by ionospheric dynamo currents. *Space Science Reviews*, *206*, 299–405.